Numerical Prediction of Microstructure and Hardness in Multicycle Simulations

A.S. Oddy and J.M.J. McDill

Thermal-microstructural predictions are made and compared to physical simulations of heat-affected zones in multipass and weaved welds. The microstructural prediction algorithm includes reaustenitization kinetics, grain growth, austenite decomposition kinetics, hardness, and tempering. Microstructural simulation of weaved welds requires that the algorithm include transient reaustenitization, austenite decomposition for arbitrary thermal cycles including during reheating, and tempering. Material properties for each of these phenomena are taken from the best available literature. The numerical predictions are compared with the results of physical simulations made at the Metals Technology Laboratory, CANMET, on a Gleeble 1500 simulator. Thermal histories used in the physical simulations included single-pass welds, isothermal tempering, two-cycle, and three-cycle welds. The two- and three-cycle welds include temper-bead and weaved-weld simulations. A recurring theme in the analysis is the significant variation found in the material properties for the same grade of steel. This affected all the material properties used including those governing reaustenitization, austenite grain growth, austenite decomposition, and hardness. Hardness measurements taken from the literature show a variation of ±5 to 30 HV on the same sample. Alloy differences within the allowable range also led to hardness variations of ±30 HV for the heat-affected zone of multipass welds. The predicted hardnesses agree extremely well with those taken from the physical simulations. Some differences due to problems with the austenite decomposition properties were noted in that bainite formation was predicted to occur somewhat more rapidly than was found experimentally. Reaustenitization values predicted during the rapid excursions to intercritical temperatures were also in good qualitative agreement with those measured experimentally.

Keywords
2.25Cr-1Mo, microstructure, prediction, tempering, welding

1. Introduction

REPAIR welding of 2.25Cr-1.0Mo steels without postweld heat treatment has been the subject of a number of long-standing research programs. During repair welding, the thermal history of the first pass creates a hard martensitic structure in the coarse-grained heat-affected zone (CGHAZ). Hydrogen-induced cracking in this location is a strong possibility unless corrective measures are taken. One method has been the reduction of the local hardness to below 250 HV through postweld heat treatment of the welded structure. This is expensive and inconvenient to apply in situ. The development of temper-bead and weaved-weld techniques to avoid this has been the subject of many experimental studies. If numerical procedures could be developed that accurately predict the effects of multiple thermal cycles, then the search for successful techniques could be shortened and the expense reduced.

A.S. Oddy and **J.M.J. McDill,** Mechanical & Aerospace Engineering, Carleton University, Ottawa, Canada.

Nomenclature

A	Tempering pre-exponential factor	H	Hardness, HV
A_{e1}	Equilibrium austenite start temperature, °C	H_∞	Fully-softened reference hardness, HV
A_{e3}	Equilibrium austenite completion temperature, °C	k	Pre-exponential grain growth factor
B	Tempering rate time-constant, K log(h)	L	Larsen-Miller parameter, K log(h)
B_s	Bainite start temperature, °C	M_s	Martensite start temperature, °C
g	Austenite grain diameter, μm	n	Grain growth power
g_o	Initial austenite grain diameter, μm	Q	Grain growth activation energy, cal/mol·K
H_o	As-quenched hardness, HV	R	Universal gas constant (1.987 cal/mol·K)

Superscripts

$t + \Delta t$	Value at end of time step	t	Value of start of time step

Subscripts

B	Relevant value for bainite fraction	∞	Fully recovered reference value
P	Relevant value for pearlite fraction	α	Relevant value for ferrite fraction
o	Initial value at formation	γ	Relevant value for austenite fraction

A crucial part of microstructural predictions of multipass welding in chromium-molybdenum steels is the development of procedures to deal with the special aspects not found in typical, single-cycle weld analyses. Figure 1 shows a thermal history typical of the CGHAZ in a three-layer weld. The most obvious problem is the occurrence of multiple reaustenitization cycles. The relatively high interpass temperature leaves a retained austenite fraction that could decompose during the reheating of the second pass. For instance, for 2.25Cr-1Mo steel, the M_s temperature is 394 °C and M_{90} was 280 °C. The interpass temperature usually specified is 260 °C. This leaves an appreciable retained austenite fraction when reheating from the next weld begins. Austenite decomposition during reheating will therefore occur. The assumption in Ref 1 that austenite decomposition occurs only during cooling is no longer valid. Furthermore, intercritical reheating leads to partial austenitization and the creation of austenite fractions with elevated carbon contents. During the weaved third pass there are several, rapid excursions to intercritical ($T > A_{e1}$) and supercritical temperatures ($T > A_{e3}$). The short duration of each pulse and the rapid cooling before the next excursion ensure that the austenite fraction formed is far less than the equilibrium value computed from the peak temperature. It also follows that austenite formation will be occurring during cooling as long as $T > A_{e1}$ and the current austenite fraction is less than equilibrium. Equilibrium austenite formation models as found in Ref 1 will lead to totally erroneous predictions by overestimating the austenite formed in each excursion. A transient reaustenitization model is essential. These difficulties were addressed in Ref 2. The algorithm uses the basic relationships in Ref 1 modified to accommodate the special problems of multipass welds.

A further general problem concerns the reduction in heat-affected zone (HAZ) hardness that occurs by tempering from subsequent weld passes. Reheating of the transformation products formed in the first weld cycle causes tempering and a reduction in hardness. This is the fundamental idea behind temper-bead and weaved techniques. Inclusion of these effects in an algorithm that allows multiple cycles of austenite formation and decomposition is also essential. Problems specific to the alloy examined can also occur. When applied to steels with moderate alloy contents, the relationships described in Ref 1 can become inaccurate. Specifically, alloy-dependent coefficients for austenite grain growth and austenite decomposition kinetics must be altered for 2.25Cr-1.0Mo steels. This report concerns the additions made to allow microstructural predictions of 2.25Cr-1.0Mo steels that include tempering. The algorithm is compared with the results of physical simulations of the microstructural evolution in the CGHAZ of a 2.25Cr-1Mo weld (Ref 3-6).

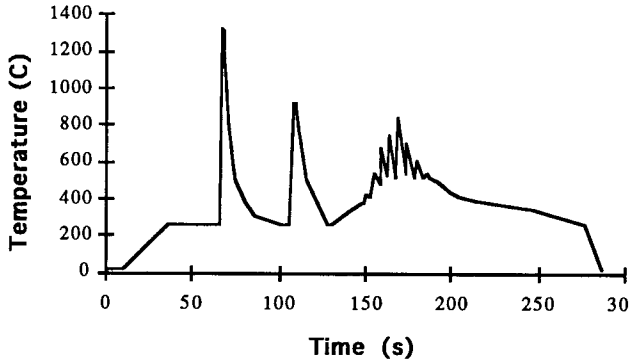

Fig. 1 Thermal history for CGHAZ of three-cycle weld

A series of material properties governs the metallurgical processes of austenite formation, grain growth, austenite decomposition, and tempering. Efforts were made to find and use the best material coefficients from the available literature. Unfortunately these properties were not always consistent when taken from different sources and in some cases conflicted with measurements made in Ref 3 to 6. Furthermore, in Ref 3 alloy differences alone are estimated to cause a difference of 30 HV in the hardness of the tempered CGHAZ. What this points to is the sensitivity of material properties to the range of allowable alloy contents within the nominal specification. Rather than alter the values to suit the measurements in Ref 3 to 6, the properties were used as taken from the sources.

2. Method

The basic structure of the microstructural prediction algorithm is essentially the same as that described in Ref 1. The ordinary differential equations (ODEs) proposed by Kirkaldy and described in Ref 1 form the basis for the underlying mathematics. When redeveloping the algorithm, modifications in Ref 2 allow austenite formation or decomposition during heating or cooling, multiple reaustenitization cycles, and transient reaustenitization. Equilibrium considerations determine austenite formation or decomposition rather than assuming only decomposition during cooling and formation during heating, as in Ref 1.The carbon content of the austenite becomes the critical factor at intercritical temperatures, and for this reason carbon content of the austenite must be tracked through the cycle of formation and decomposition. Multiple reaustenitization cycles create situations where a given phase fraction might be a mixture of old and newly formed subfractions. Careful averaging of quantities such as austenite grain size, carbon content of all phases, and hardness is essential.

The transient reaustenitization model is divided into two consecutive processes. The first is the dissolution of the iron-carbide phases and the creation of an austenite fraction of eutectoid carbon content. After the dissolution of all iron carbides, the second process, that of carbon diffusion into the remaining ferrite fractions and the conversion of that ferrite into austenite, occurs. Austenite formation begins as soon as temperatures rise above the equilibrium value A_{e1}. Rapid heating raises the apparent austenite formation temperatures A_{c1}, A_{c3} above the equilibrium values A_{e1}, A_{e3}. Predictions were compared in Ref 2 with measurements made on a SA508 cl. 3 steel. Increasing the heating rate from 1 to 70 °C/s raised the measured A_{c1} from 730 to 760 °C and the measured A_{c3} from 840 to 870 °C. Predicted values followed this closely as A_{c1} increased from 737 to 774 °C and A_{c3} from 818 to 886 °C. Considering the experimental difficulties, the agreement was quite good.

2.1 *Grain Growth*

The role of austenite grain size in the austenite decomposition kinetics is central to microstructural predictions. Austenite decomposition ODEs in Ref 1 show the strong effect of austenite grain size on kinetics. References 3 to 6 also demonstrate that multiple reaustenitization cycles can be used to refine the grain structure left in the CGHAZ of the first pass. This reaustenitization and grain refinement can convert the martensite left by the first pass into bainite. The general relation used for austenite grain growth is

$$\frac{dg}{dt} = \left(\frac{k}{ng^{n-1}}\right)\exp\left[\frac{-Q}{RT}\right] \quad \text{(Eq 1)}$$

where g is the austenite grain diameter, t is time in seconds, T is the temperature in K, Q is the activation energy for grain growth, and k is a pre-exponential factor. The terms n, k, and Q are material properties.

The experimental examination of austenite grain growth in HAZs for 2.25Cr-1Mo in Ref 7 recommended value for n quite different from the usual value of 2. From the results of physical simulations of grain growth in the HAZ of 2.25Cr-1Mo welds, Ref 7 recommended the use of

$$n = 3.17$$

$$\frac{k}{n} = 2.79 \times 10^9 \quad \text{(Eq 2)}$$

$$Q = 4.3 \times 10^4 \text{ cal/mol} \cdot \text{K}$$

for g in microns and t in seconds.

Grain growth cannot begin before the dissolution of the secondary carbides has occurred. This is accomplished in Ref 1 by preventing grain growth until temperatures exceed some precipitate dissolution temperature. This depends on the alloy and chemical species involved. For the microalloyed steels examined in Ref 1, a value of 1044 °C was used. Dilatometric tests on 2.25Cr-1Mo steel in Ref 7 involved heating to and cooling from 1100 °C at various rates. Austenite grain sizes of 13 to 25 μm were measured, indicating that the dissolution temperature was below 1100 °C. Therefore, 1044 °C was kept as the precipitate dissolution temperature for 2.25Cr-1Mo steel.

Grain growth, like every other physical process, is affected by material properties that vary with alloy content. Some of the grain growth results presented in Ref 7 appear to be in conflict with measurements reported in Ref 3 and 4 and micrographs presented in Ref 5 and 6. Comparisons are difficult; however, prior austenite grain diameters for heavier welds (≥1.1 kJ/mm) in Ref 7 are substantially smaller than those found in Ref 3 to 6 for peak temperatures of approximately 1350 °C These comparisons are scarcely conclusive, but are indicative of potential differences. The most likely explanation is that small differences in alloy content are affecting the austenite grain growth. In spite of these potential difficulties, the austenite grain growth equations in Ref 7 were adopted for this investigation.

2.2 *Austenite Decomposition Kinetics*

A series of ODEs are used in Ref 1 to describe the kinetics of ferrite, pearlite, and bainite formation from austenite. Polynomial equations are used to describe the alloy dependence of these terms. Although the results are very good for a range of low-alloy steels, they become increasingly inaccurate for higher alloy contents. This is especially true for alloys where a secondary austenite bay opens between the ferrite and bainite start lines. The 2.25Cr-1Mo steels certainly fall into this category as Ref 8 demonstrates.

Extraction of the relevant coefficients from an isothermal transformation diagram is a trivial exercise. The coefficients used in this investigation for the austenite decomposition kinetics of 2.25Cr-1Mo steel were taken from Ref 8. Figure 2 shows the resulting isothermal transformation diagram when the specific coefficients extracted from Ref 8 are used in the ODEs from Ref 1. The prior austenite ASTM grain size is 5 to 6 (approximately 60 μm diameter).

Evidence of some sensitivity to alloy content can be found in many sources. In Ref 6, alloy differences for two samples, both nominally SA387 Gr. 22 steels, caused a 30 HV difference in hardness after three weld cycles. Additional citations in Ref 8 for other examples of 2.25Cr-1Mo steels show that the equilibrium critical temperatures also vary considerably; for example:

$$871\ ^\circ\text{C} \le A_{e3} \le 900\ ^\circ\text{C}$$

$$728\ ^\circ\text{C} \le A_{e1} \le 804\ ^\circ\text{C}$$

$$528\ ^\circ\text{C} \le B_s \le 600\ ^\circ\text{C} \quad \text{(Eq 3)}$$

$$380\ ^\circ\text{C} \le M_s \le 420\ ^\circ\text{C}$$

The values used in this investigation for the critical temperatures were $A_{e3} = 871$ °C, $A_{e1} = 804$ °C, $B_s = 528$ °C, $M_s = 394$ °C. These are the values obtained from Ref 8, but again they appear to conflict with data in Ref 3, where $A_{e1} \le 780$ °C.

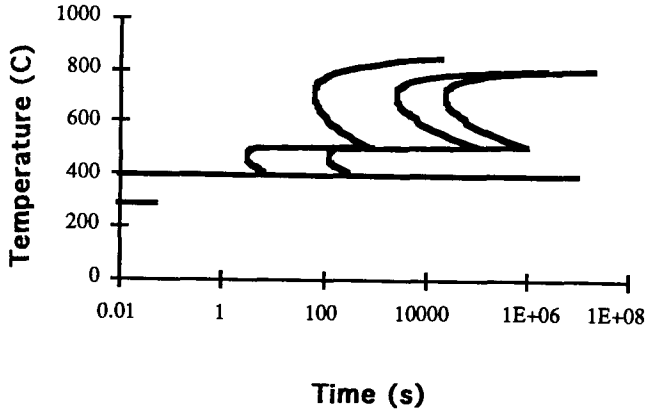

Fig. 2 Isothermal transformation diagram for 2.25Cr-1Mo steel (grain size: 5 to 6). Source: Ref 8

2.3 *Tempering and Hardness*

Temper-bead and weave welding techniques are intended to replace postweld heat treatment as the means of reducing the HAZ hardness. These techniques share a common process in that reheating tempers and softens the HAZ left by the first layer. Including these effects in a numerical model requires the solution of three problems. First, the degree of tempering must be related to measurable quantities such as hardness. Second, softening rates must be defined in terms of time and temperature. There do not appear to be universally accepted relationships strongly rooted in metallurgical theory for each of these problems (Ref 9). Finally, whatever relationships are used, each requires material properties to describe different alloys. Various relationships exist in the literature that attempt to relate tempering, time, and temperature (Ref 9). At best, only empirical relationships are available. Graphical formats as in Ref 10 adapt poorly to numerical techniques. In Ref 11, three different empirical relationships are used to describe the softening that occurs during reheating of an SA508 cl. 2 steel. Different relationships are required for different initial hardnesses. Given these problems and the probable sensitivity to variations in alloy content, the use of a simple relationship seemed justified.

The first difficulty in including the effects of tempering lies in describing the state of recovery to changes in physically measurable quantities like hardness. Given that initial, as-quenched hardnesses may vary, having individual tempering relationships for each initial value is inconvenient. The hardness changes will be described by defining a dimensionless or normalized relationship for the degree of softening

$$\Phi = \frac{H_0 - H(t)}{H_0 - H_\infty} \qquad \text{(Eq 4)}$$

where H_0 is the initial, as-quenched hardness; H_∞ is the fully softened reference value; $H(t)$ is the tempered hardness at time t. This has many advantages in that data for different initial hardnesses can be compared and a dimensionless term appears. All three empirical relations in Ref 11 can be collapsed into a single relation when this transformation is applied (Ref 12).

Simple, thermally activated rate equations are used to justify the Larsen-Miller or Holloman-Jaffe parameter as the relevant term to describe the tempering process. For isothermal treatments,

$$L = 1.8(T + 273)(20 + \log(t)) \qquad \text{(Eq 5)}$$

for T in °C and t in hours. This has several important implications that can be in conflict with experimental measurements, but it is arguably the best available (Ref 9) and when used in empirical relations makes an adequate fit. For anisothermal treatments, a pseudotime summation scheme (Ref 12) is more rapid than the numerical integration of the relevant ODE. In Ref 11 and elsewhere, experiments show that the rate of hardness reduction increases as L and Φ increase. The simplest ODE for circumstances of this type is

$$\frac{d\Phi}{dL} = \frac{\Phi}{B} \qquad \text{(Eq 6)}$$

where B is a material parameter. The solution for this ODE is

$$\Phi = A \exp\left[\frac{L}{B}\right] \qquad \text{(Eq 7)}$$

Specifically,

$$\frac{H_0 - H(t)}{H_0 - H_\infty} = A \exp\left[\frac{L}{B}\right] \qquad \text{(Eq 8)}$$

where A and B are material properties and L is the Larsen-Miller or Holloman-Jaffe parameter.

The tempering relation adopted includes only the softening during tempering. Secondary hardening due to precipitation of additional carbides is not included. In Ref 12, tempering data for SA508 cl. 2 steel were taken from Ref 11 and 13, summarized, and found to be extremely well described by Ref 9:

$$\frac{H_0 - H(t)}{H_0 - H_\infty} = A \exp\left[\frac{L}{B}\right] \qquad \text{(Eq 8)}$$

This relation proved to be exceptionally convenient. Using only two material coefficients, it made accurate predictions of tempered hardnesses for initial hardnesses ranging from 300 to 450 HV, and for tempering temperatures ranging from 300 to 700 °C (Ref 12).

This basic relationship was again adopted to describe tempering in 2.25Cr-1Mo steels. The isothermal results in Ref 5 were used to determine appropriate values for A and B. For 2.25Cr-1Mo steel, time in hours and temperature in °C, the values obtained were

$$A = 0.0053$$

$$B = 7290 \qquad \text{(Eq 9)}$$

For martensite, the as-quenched hardness was $H_0 = 418$, the as-quenched hardness for bainite was $H_0 = 350$, and the fully softened reference value was $H_\infty = 200$. Using these relationships to describe tempering behavior has the chief advantages of simplicity and convenience. Figure 3 compares the tempering behavior predicted for initially martensitic structures using this relationship with the isothermal tempering results from Ref 5 to show how well the relationships can fit measurements. Also shown for comparison are the values predicted with the empirical method described in Ref 10. The proposed numerical relationship provides a good fit with both the experimental results in Ref 5 and the empirical predictions of Ref 10.

The tempering equation must be integrated with a multicycle austenite formation/decomposition model. Reaustenitization and decomposition constantly create a mixture of as-quenched and tempered martensite and bainite. Averaging

procedures are required to avoid a proliferation of data structures. They must still meet the basic conditions that heating without reaustenitization causes softening, but formation of fresh bainite and martensite increase the hardness. This was accomplished by allowing two opposing trends to affect L. The value of L increases as reheating tempers the microstructure. On the other hand, L decreases as fresh martensite and bainite form and hardness increases.

A linear law of mixtures rule is used to describe the hardness of the mixture of phases:

$$H^{t+\Delta t} = H_\infty\left(x_\gamma^{t+\Delta t} + x_\alpha^{t+\Delta t} + x_P^{t+\Delta t}\right) + H_B^{t+\Delta t}x_B^t + H_{Bo}\Delta x_B + H_M^{t+\Delta t}x_M^t + H_{Mo}\Delta x_M \quad \text{(Eq 10)}$$

Individual terms represent the contribution of the austenite, ferrite, and pearlite fractions $H_\infty(x_\gamma^{t+\Delta t} + x_\alpha^{t+\Delta t} + x_P^{t+\Delta t})$; the tempered hardness of the bainite and martensite that existed at the beginning of the time step; that is, $H_B^{t+\Delta t}x_B^t$ and $H_M^{t+\Delta t}x_M^t$; and the contribution of bainite and martensite freshly formed in the step; that is, $H_{Bo}\Delta x_B$, and $H_{Mo}\Delta x_M$.

The hardness of the tempered bainite fraction x_B^t and tempered martensite fraction x_M^t; are computed from

$$H_B^{t+\Delta t} = H_{Bo} - (H_{Bo} - H_\infty)A\exp\left[\frac{L^{t+\Delta t}}{B}\right]$$

$$H_M^{t+\Delta t} = H_{Mo} - (H_{Mo} - H_\infty)A\exp\left[\frac{L^{t+\Delta t}}{B}\right] \quad \text{(Eq 11)}$$

where $L^{t+\Delta t}$ is computed by integrating over the time step or through a pseudotime summation. It increases as long as some bainite of martensite fraction exists.

Formation of fresh bainite or martensite requires some type of reduction or resetting of the value for $L^{t+\Delta t}$. Maintaining manageable data structures requires an averaging process. This enables single parameters to represent the mixture of old and new microstructural components. Tempering is assumed not to affect the hardness of the austenite, ferrite, and pearlite components. The untempered hardness of the bainite/martensite mixture is computed from

$$H_o^{t+\Delta t} = \frac{H_{Mo}x_M^{t+\Delta t} + H_{Bo}x_B^{t+\Delta t}}{x_M^{t+\Delta t} + x_B^{t+\Delta t}} \quad \text{(Eq 12)}$$

and the current hardness of the tempered mixture of bainite and martensite is computed from

$$H_{BM}^{t+\Delta t} = \frac{H_B^{t+\Delta t}x_B^t + H_{Bo}\Delta x_B + H_M^{t+\Delta t}x_M^t + H_{Mo}\Delta x_M}{x_B^{t+\Delta t} + x_M^{t+\Delta t}} \quad \text{(Eq 13)}$$

From these values for the untempered and tempered bainite/martensite mixtures, an average value for $L^{t+\Delta t}$ is computed. This reflects the readjustment that must occur as fresh bainite and martensite form:

$$L^{t+\Delta t} = B\left[\ln\left(\frac{H_o^{t+\Delta t} - H_{BM}^{t+\Delta t}}{H_o^{t+\Delta t} - H_\infty}\right) - \ln(A)\right] \quad \text{(Eq 14)}$$

The overall process is therefore divided into two subprocesses. Time and temperature, regardless of whether or not any austenite formation or decomposition occurs, causes an increase in the value for $L^{t+\Delta t}$ and some resultant tempering. Formation of new bainite and martensite increases the averaged or mixed hardness, which reduces the value of $L^{t+\Delta t}$.

2.4 *Material Properties*

Metallurgical predictions in multiple thermal cycles require the successful integration of at least five processes. Material properties describe the response of an alloy to each of these processes. It follows that these processes do not occur independently of one another. Some strongly influence the subsequent effects of others even if they do not occur simultaneously. For example, austenite grain growth influences the austenite decomposition kinetics, which in turn has a strong effect on the hardness. In order of relative importance, the metallurgical processes modeled in this investigation are:

1. Austenite grain growth kinetics
2. Austenite decomposition kinetics
3. Hardness of austenite decomposition products
4. Tempering of bainite and martensite fractions
5. Reaustenitization

Even if the algorithm were perfect and the mathematical expressions used were without simplifying assumptions, any errors in the material properties used would have a direct effect on the predictions made. Material properties were collected from several sources. The alloy content varied somewhat within the nominal range. Austenite grain growth properties were taken from Ref 7. Austenite decomposition properties were taken from Ref 8. As-quenched hardness values were taken from Ref 3 to 6, and tempering properties from Ref 5.

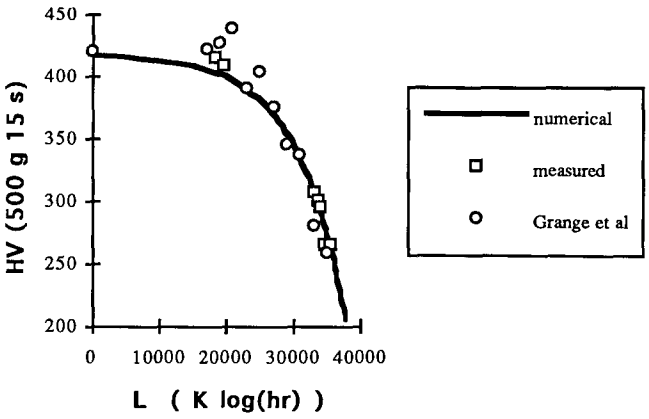

Fig. 3 A comparison of numerical, experimental, and empirical hardness (Ref 10) after tempering

Reaustenitization kinetics and properties followed the method outlined in Ref 2.

Given the sensitivity of the properties to variations in the content, it is a fair question to ask if the collection is representative of anything at all. That can only be judged by comparing predictions made with the model to experimental measurements from physical simulations found in Ref 3 to 6. A perspective on what constitutes a good correlation can be gained from Ref 3 to 6 where multiple hardness measurements on the same sample revealed an experimental error ranging from ±5 to ±30 HV. Furthermore, in Ref 4, alloy differences alone are estimated to cause as much as 30 HV differences in the CGHAZ hardness of three-layer welds.

3. Results

The results of physical simulations of CGHAZ microstructure make an ideal source of experimental data to evaluate the predictive algorithm presented here. Thermal histories were taken from the physical simulations made at MTL/CANMET using the Gleeble 1500 thermal-mechanical weld simulator (Ref 3-6). This body of experimental measurements is comprehensive, including single-cycle welds and isothermal tempering tests, as well as multicycle, temper-bead, and weaved-weld simulations. Table 1 briefly describes the tests.

Predicted austenite grain diameters in the single-weld simulations are quite small, on the order of only 20 to 24 μm. This is comparable to the measurements in Ref 7, but considerably smaller than the micrographs in Ref 3 to 6 would suggest. Although no values are quoted, the micrographs certainly suggest values much larger than 30 μm.

The two- and three-cycle weld predictions are interesting from several perspectives. First, with M_s equal to 394 °C, M_{90} equal to 305 °C, and the interpass temperature at 260 °C, the Koistinen-Marburger equation predicts that a retained austenite fraction of 7% exists at the start of the second weld cycle. This austenite fraction will decompose during the reheating of the second cycle.

The weaved second and third thermal cycles involve repeated excursions into the intercritical range where some reaustenitization occurs, but much less than equilibrium calculations would suggest. For example, for peak temperatures of 810, 830, and 860 °C, equilibrium calculations would predict austenite fractions of 24, 35, and 72%, respectively. This is far more than was observed. The fractions predicted to form by the transient austenite formation model used in this investigation depend not only on the peak temperature, but also on the heating and cooling rates. Nevertheless, predicted austenite fractions were much lower than the equilibrium values. No appreciable austenite formation occurred in the second cycle for either RBW2 (1350, 810 °C weaved) or RBW5 (1350, 840 °C weaved). For RBW4 (1350, 860 °C weaved), only 6% austenite formed in the second cycle.

Figure 4 shows the correlation between predicted and measured hardness from these tests. When evaluating the accuracy of the numerical model, it is useful to recall that hardness measurements made on the same specimen vary by as much as ±30 HV from the listed values (Ref 3-6). This variation occurs in spite of the most careful control and demonstrates the inherent variability of the physical processes involved. In fact, Ref 4 estimates that a further ±30 HV variation exists simply as a result of the composition differences present within the nominal alloy specification. The correlation between measured and predicted values is, therefore, excellent.

Points lying above the 1-to-1 correlation line represent nonconservative predictions; that is, predicted hardnesses are less than those measured. While most points are below or only slightly above the line, there are two points that lie significantly above the 1-to-1 correlation. One is from a two-cycle weld simulation, and the other is for a three-cycle weld simulation. Both points share a common characteristic in that the second cycle is a weaved weld with a peak temperature of 910 °C. In both cases, complete reaustenitization occurs, but the slow cooling of the weaved cycle leads to a prediction of 100% bainite formation. The experimental results show a mixed microstructure of bainite and martensite. The bainite formation kinetics used in the prediction appear to be slightly too rapid.

Table 1 Thermal cycles in physical simulations

Sample ID	Type	Thermal cycle peak temperatures, °C		
		Cycle 1	Cycle 2	Cycle 3
RBP1	Single weld $\Delta t_{800/500}$ = 4.6 s	1350	...	...
RBP2	Single weld $\Delta t_{800/500}$ = 2.2 s	1350	...	...
RBH2	Isothermal temper	1350	30 s at 750 °C	...
RBH	Isothermal temper	1350	60 s at 750 °C	...
RBH3	Isothermal temper	1350	90 s at 750 °C	...
RBH4	Isothermal temper	1350	600 s at 750 °C	...
RBH5	Isothermal temper	1350	750 s at 720 °C	...
RBW3	Two-cycle weld	1350	760 °C weaved	...
RBW6	Two-cycle weld	1350	790 °C weaved	...
RBW2	Two-cycle weld	1350	810 °C weaved	...
RBW5	Two-cycle weld	1350	840 °C weaved	...
RBW4	Two-cycle weld	1350	860 °C weaved	...
RBW1	Two-cycle weld	1350	910 °C weaved	...
RB3C	Three-cycle weld	1350	770 °C	830 °C weaved
RB3B	Three-cycle weld	1350	860 °C	830 °C weaved
RB3A	Three-cycle weld	1350	860 °C weaved	830 °C weaved
RB3D	Three-cycle weld	1350	910 °C	830 °C weaved
RB3E	Three-cycle weld	1350	910 °C weaved	830 °C weaved

This is probably due to austenite decomposition coefficients differing slightly from the true values. On the other hand, measurements (Ref 4) and calculations agree that for a peak temperature of 1350 °C, the HAZ is fully martensitic for 800 to 500 °C cooling times of less than 6 s. Furthermore, the same algorithm and same coefficients were used in Ref 14,where computed bainite transformation rates were slower than measured. These apparent inconsistencies would again point to some sensitivity to alloy content, even within the nominal range. The differences in material properties are probably not large. Only a small change might be required to change the predicted fully bainitic structure to a mixed bainitic/martensitic structure. Overall, the agreement between the predicted and measured hardness is excellent.

The final microstructure for the intercritically reheated specimen RBW2 (1350, 810 °C weaved) was predicted to be 92% tempered martensite and 8% bainite. The bainite fraction came from two sources: 4% came from austenite decomposition during reheating and the remainder from austenite decomposition during the cooling half of the second weld cycle. No reaustenitization was predicted during the excursion to 810 °C. Martensite created in the first cycle was tempered in the second cycle. The predicted hardness was 329 HV. The measured hardness was 296 ± 11 HV. The microstructure was described as predominantly a tempered martensite with a small fraction of transformation product from reaustenitization at the grain boundaries. The value assumed for A_{e1} will have a direct bearing on the reaustenitization calculations. As previously discussed, the value chosen may well be greater than the actual value for the specimen used.

Another intercritical specimen RBW4 (1350, 860 °C weaved) was predicted to have a final microstructure of 87% tempered martensite and 13% bainite, with a final hardness of 302 HV. The excursion to 860 °C spent 2.6 s above A_{e1}. The approximately 5% austenite fraction remaining from the first weld increased to 11% during the excursion to 860 °C; that is, 6% reaustenitized fraction. The majority of the austenite present formed bainite during the final cooling. The measurements made on this specimen showed a final hardness of 318 ± 12 HV. The tempered martensite fraction was 296 HV, whereas the grain boundary bainite, formed from the reaustenitized fraction was 347 HV. The volume fraction of new austenite forming on the grain boundaries was not estimated in Ref 5 or 6, but, judging from the micrographs, cannot have been large and must be roughly comparable to the 6% value predicted.

The specimen RBW1 (1350, 910 °C weaved) was fully reaustenitized in the second weld cycle of the numerical simulation. The predicted final microstructure was 94% bainite and 5% martensite, with a hardness of 339 HV. This contrasts somewhat with the physical simulation where a mixed bainite/martensite microstructure with a hardness of 374 ± 10 HV was observed. The relative amounts of bainite and martensite observed were not measured, but presumably show less bainite and more martensite than predicted. As has been discussed already, the numerical prediction seems to overestimate the bainite transformation rate. This is most likely due to inaccuracies in the austenite decomposition properties that were used. Small changes may be all that are required to bring the relative fractions into better agreement.

In the three-cycle simulations, RB3A (1350, 860 °C weaved, 830 °C weaved) can be compared with RB3B (1350, 860, 830 °C weaved) to show the sensitivity of the austenite formation kinetics to small differences in the thermal history. The weaved second cycle in RB3A showed very little reaustenitization, only slightly more than 1%. In RB3A, the time spent above A_{e1} was approximately 1.06 s. The temper-bead second cycle in RB3B shows more austenite formation, with approximately 6% new austenite forming. In RB3B, the second temper-bead cycle spent approximately 1.64 s above A_{e1}. This shows how sensitive the reaustenitization kinetics are to small changes in the thermal cycle. Austenite formation is known to occur very rapidly. Experimental investigations of austenite formation will require stringent control of the thermal history above A_{e1}.

Comparing the predictions for RB3A (1350, 860 °C weaved, 830 °C weaved) to experiment shows predicted hardnesses and reaustenitized fractions close to but slightly below measured values. The predicted final hardness was 302 HV for a mixture of 91% tempered martensite and 9% bainite. Very little reaustenitization, approximately 1%, was predicted for the second, weaved, thermal cycle. No new austenite was predicted for the third cycle. Measured values for this specimen indicated a final hardness of 305 ± 11 HV. Reaustenitization occurring at the grain boundaries left a mixed bainite/martensite after the second cycle with some further reaustenitization occurring in the third cycle. The amounts formed were very small, existing as only very thin layers on the grain boundaries. The differences between the predicted and measured behavior are very small.

Similar results are evident for RB3B (1350, 860, 830 °C weaved). The predicted final hardness was 304 HV from a mixture of 92% martensite and 8% bainite. The martensite fraction itself was predominantly tempered martensite (85%). Approximately 5% martensite formed between the second and third weld cycles with a further small component (1%) predicted to form after the third weld cycle. While some bainite was predicted during the second cycle, most formed during the third cycle. Reaustenitization primarily occurred only in the second weld cycle when 6% austenite formed. Only 0.1% austenite was predicted to form in the third weld cycle. A sizable austenite fraction (5%) retained from the second cycle was carried through the reheating of the third cycle before finally van-

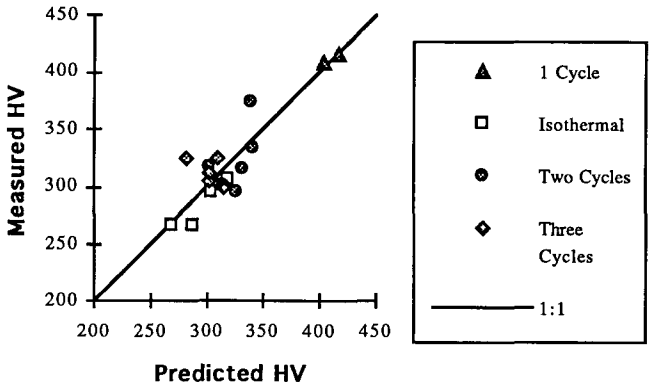

Fig. 4 Predicted versus measured hardness in physical simulations

ishing during cooling. This agrees well with the physical simulation where reaustenitization of a thin layer at the grain boundaries during the second cycle formed martensite. This was followed by some further reaustenitization of a smaller fraction in the third cycle. The final microstructure was a tempered martensite surrounded by a grain boundary layer of bainite and martensite. The final measured hardness was 305 ± 13 HV. Thus, the principal difference between the predicted and measured values was the very small amount of reaustenitization predicted in the third cycle.

Somewhat larger differences exist between the predicted and measured results for RB3E (1350, 910 °C weaved, 830 °C weaved). The predicted history shows complete reaustenitization during the second cycle with a mixture of 95% bainite and 5% martensite forming in that cycle. The predicted prior austenite grain size in the second cycle is very small, only 10 μm in diameter, because temperatures do not exceed the assumed precipitate dissolution temperature. Predictions for the third cycle show no reaustenitization, only tempering, leaving a final hardness of 282 HV. In contrast to this, while the physical simulations also show complete reaustenitization in the second cycle, the decomposition products were a mixture of bainite and martensite. The third cycle is reported to produce a tempered martensite with a network of bainite and martensite at the grain boundaries. The final hardness was 324 ± 16 HV. The difference between the predicted and measured hardness is caused mainly by the fact that more bainite is predicted to form in the second cycle than was actually found in the physical simulation. As already discussed, this may be due to the sensitivity of the decomposition properties to variations in alloy content.

A final word on transient austenite formation concerns the sensitivity of austenite formation to the peak temperature. Small changes in the value for the peak temperature cause large differences in the austenite fraction formed. For instance, changing the peak temperature from 910 to 902 °C lowers the austenite fraction formed from 100 to only 25%. This clearly illustrates the exceptional control required if any experimental studies are to be undertaken.

4. Conclusions

Material properties taken from published sources show considerable variation for alloys that fall within the nominal composition for 2.25Cr-1.0Mo steel. In some cases, values from different sources are contradictory.

Variations in material properties lead directly to substantial variations in any measured quantity associated with the microstructure. Alloy variations alone are reported to cause a 30 HV difference in hardnesses measured after multipass welding. Hardnesses measured on single samples typically show hardness variations of ±5 HV, rising in extreme cases to ±30 HV. The accuracy of any predictions must be judged in the light of this experimental error.

The proposed empirical tempering relation can make a good fit to the experimental measurements and is in good agreement with the empirical predictive method described in Ref 10 for this material.

Comparisons of predicted and measured hardnesses for physical simulations of single-pass welds, isothermal tempering, and multipass temper-bead or weaved welds are in excellent agreement. Some results indicate that bainite formation rates are overestimated to some degree in the predictions. The effects of alloy variations on the material properties are suspected as the cause.

Acknowledgments

The support of the Metals Technology Laboratory, CANMET, and NSERC Operating Grant 41745 are gratefully acknowledged.

References

1. D.F. Watt, L. Coon, M. Bibby, J. Goldak, and C. Henwood, An Algorithm for Modeling Microstructural Development in Weld Heat-Affected Zones, Part A, *Acta Metall.*, Vol 36 (No. 11), 1988, p 3029-3035
2. A.S. Oddy, J.M.J. McDill, and L. Karlsson, Microstructural Predictions Including Arbitrary Thermal Histories, Reaustenitization, and Carbon Segregation Effects, submitted *Can. Metall. Q.*, March 1995
3. J.T. Bowker, J.T. McGrath, R.F. Orr, M.W. Letts, and T.W. Lau, "Temper-Bead Repair in Cr/Mo Steels," MTL 91-16(OP-J), IIW Doc.IX.1633.91, Metals Technology Laboratory, Ottawa, Canada
4. T.W. Lau and D. Hartwick, "Weave Welding Techniques: Their Effects on the Microstructure and Hardness of 2¼Cr-1Mo Steels," OHRD Report M91-61-K, Ontario Hydro Research Division
5. R.J. Bowers and M.W. Letts, "Weld-Repair Simulation in 2.25Cr-1Mo Steel," MTL 94-11(J), Metals Technology Laboratory, Ottawa, Canada
6. R.J. Bowers, M.W. Letts, R.F. Orr, J.E.M. Braid, T.W. Lau, and D.B. Hartwick, Weld Repair of 2.25Cr-1Mo Pressure Vessel Steel, *Proc. of Int. Symp. Mater. Performance, Maintenance and Plant Life-Assessment* (Toronto, Ont.), Metallurgical Society of CIM, Aug 1994, p 193-205
7. R.M. Miranda and M.A. Fortes, Austenite Grain Growth, Microstructure and Hardness in the Heat-Affected Zone of a 2.25Cr-1Mo Steel, *Mater. Sci. Eng.*, Vol A108, 1989, p 1-8
8. G.F. Vander Voort, Ed., *Atlas of Time-Temperature Diagrams for Iron and Steel*, ASM International, 1991, p 484
9. S. Murphy and J.H. Woodhead, An Investigation of the Validity of Certain Tempering Parameters, *Metall. Trans.*, Vol 3, 1972, p 727-735
10. R.A. Grange, C.R. Hribal, and L.F. Porter, Hardness of Tempered Martensite in Carbon and Low-Alloy Steels, *Metall. Trans. A*, Vol 8A, 1997, p 1775-1785
11. P.J. Alberry, Computer Model for Multipass Repair Welds in SA508 Class 2 Alloy, *Weld. J.*, Vol 68 (No. 10), 1989, p 410s-417s
12. R.S. Chandel and A.S. Oddy, An Algorithm for the Prediction of Hardness of Repair Welds in 2.25Cr-1Mo Pressure Vessel Steel—A Preliminary Study, *Pressure Vessel and Piping Technology Seminar* (Singapore), ASME Press, May 1993, p 433-439
13. P.J. Alberry and J.A. Lambert, The Welding Metallurgy of SA508 Cl II Heat Affected Zones, *Int. Conf. Welding Technology for Energy Applications* (Gatlinburg, TN), ASM International, May 1992, p 347-369
14. L.E. Lindgren and A.S. Oddy, Toolbox for Computing Phase Transformations and Material Properties of Hypoeutectoid Steels in Satoh Test, *First Int. Symp. on Thermal Stresses and Related Topics* (Hamamatsu, Japan), 5-7 June, 1995